Anal Bioanal Chem (2016) 408:2813–2825
DOI 10.1007/s00216-015-9203-3

REVIEW

Optical sensing and biosensing based on non-spherical noble metal nanoparticles

Yunsheng Xia [1]

Received: 29 September 2015 / Revised: 13 November 2015 / Accepted: 18 November 2015 / Published online: 9 December 2015

Abstract Non-spherical noble metal nanoparticles (NPs) have widely tunable localized surface plasmon resonance, very high extinction coefficient, and strongly facet-dependent adsorption/binding properties. A few non-spherical noble metal NPs have been employed as reporters and/or modulators for various optical sensing. This review summarizes recent progress in the study of design, performance, and application of colorimetric and fluorescent sensing/biosensing systems based on three kinds of non-spherical noble metal NPs with different dimension, namely, one- (or quasi-one) dimensional nanorods, two-dimensional nanoplates, and three-dimensional nanodendritics; furthermore, the future developments in this research area are also discussed.

Keywords Sensing · Biosensing · Optical sensors · Non-spherical metal nanoparticles

Background

In the last 30 years, the remarkable achievements in nanoscience and nanotechnology well promote the development of analytical chemistry. Various nanomaterials with special optical, electrical, and magnetic properties possess great potential applications in detection, imaging, separation, enrichment, etc. [1–12]. Especially, noble metal (eg., Au, Ag) nanoparticles (NPs) have attracted considerable attention in sensing/biosensing applications because of their prominent optical property, versatile surface modification chemistry, and multiple signal output modes [13–21]. Since surface-modified Au NPs were employed as colorimetric reporters for studying DNA hybridization [22, 23], noble metal NP-based systems have been well explored and constructed for the detection of multifarious target analytes. Noble metal NP-based detection systems have been well studied and obtained many significant results. In recent year, a few excellent reviews on this field have been published [13–21]. However, to our knowledge, there is no review paper that has focused on the design, performances, and sensing/biosensing applications of non-spherical metal NPs. In terms of noble metal NPs, there are several features on size/shape influenced physicochemical properties. First, compared with semiconductor NPs [quantum dots, (QDs)] [24], the optical bands of noble metal ones are less size-dependent. As shown in Fig. 1a, the localized surface plasmon resonance (LSPR) peaks of spherical Au NPs remain almost unchanged in the size range from 2.5 to 14 nm [26]. In contrast, the LSPR bands of rod-like NPs can be easily tuned from visible to near-infrared region by their aspect ratio (Fig. 1d) [27, 28]. In this regard, the latter is more appropriate and versatile as energy acceptors in the construction of fluorescence resonance energy transfer (FRET) systems. Then, metal NPs with specific shape possess higher extinction coefficient. For example, the extinction coefficient of Au and Ag rod NPs is as high as 10^9 to 10^{11} M^{-1} cm^{-1}, which is much higher than those of spherical NPs [29–31]. As we know, toward colorimetric system, a higher extinction coefficient of the used reporters facilitates enhancing the sensitivity [32]. Third, anisotropic metal NPs have certain exposed facets, which can cause preferential binding, adsorption, as well as self-assembly

Published in the topical collection featuring *Young Investigators in Analytical and Bioanalytical Science* with guest editors S. Daunert, A. Baeumner, S. Deo, J. Ruiz Encinar, and L. Zhang.

✉ Yunsheng Xia
xiayuns@mail.ahnu.edu.cn

[1] Key Laboratory of Functional Molecular Solids, Ministry of Education, College of Chemistry and Materials Science, Anhui Normal University, Wuhu 241000, China

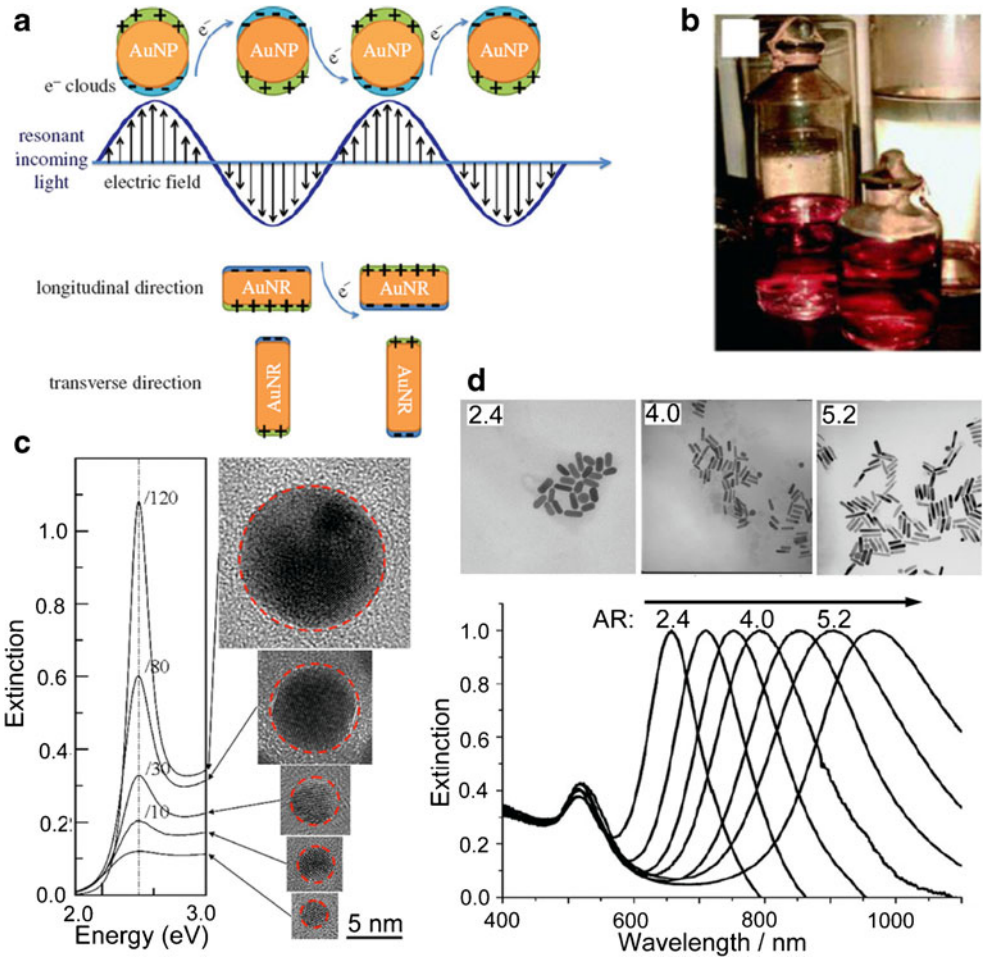

Fig. 1 Optical property of Au NPs. (**a**) Surface plasmon oscillations in spherical gold NPs and AuNRs. (**b**) Au NPs in Faraday's colloidal samples. (**c**) LSPR bands of different sized Au NPs. (**d**) TEM images and LSPR bands of AuNRs with different aspect ratio; Figure reprinted with permission from Refs. [20, 25–27], respectively

behaviors. These properties are very significant for better analytical performances (enhance sensitivity and/or selectivity) [33, 34]. Lastly, a few NPs have special superstructures (dendritic, star, flower, etc.), and their extremely strong electromagnetic field resulting from coupling effect can well heighten various molecular spectroscopy applications, including fluorescence, infrared absorption, and Raman scattering [35–37]. As a result, powerful sensing systems can be constructed accordingly. Because of these reasons, non-spherical metal NPs possess many advantages over spherical ones in sensing/biosensing applications.

Without a doubt, the controllable synthesis of nanomaterials has made great progresses on account of the consistent efforts of chemists and material scientists. For example, various semiconductor and metal NPs with tunable size can be well synthesized by bottom-up strategies, and their size distribution is as low as 5 % [38–40]. In addition to spherical and quasi-spherical products, various nanomaterials with more complicated morphology and/or structure, such as rod-, wire-, plate-, star-like, etc. can also be obtained by combination of thermodynamics and dynamics regulation [27–30, 33, 41–43]. These studies, on the one hand, are the interest of synthetic chemistry; on the other hand, these studies well extend the properties and applications of various nanomaterials.

In this review, we summarize the state-of-the-art progress in the design, performances, and applications of optical sensing/biosensing systems using non-spherical metal NPs as reporters and/or modulators. The review discusses three kinds of non-spherical metal NPs with different dimension, namely, one- (or quasi-one) dimensional nanorods, two-dimensional nanoplates, and three-dimensional nanodendritics. Before the summary, the optical properties of noble metal NPs are briefly introduced, considering that they will be intensively mentioned in this review. At the end of this review, the prospects of non-spherical NP-based sensing/biosensing will also be discussed. Several points should be noted here. First, the signal readout modes are focused on colorimetry and fluorescence. Raman scattering, including surface enhanced Raman scattering (SERS), is not included because of the following reasons. Generally, the quantitative SERS measurements are rather difficult [44] although they possess ultrahigh sensitivity and hold promise for sensing/biosensing applications. On the other hand, there have already been several excellent reviews that are focused on metal NPs-based SERS systems [45, 46], and they contain a

few shape-related properties. The interested reader can consult these publications. Second, the discussed fluorescence arises from extrinsic fluorophores; and the intrinsic fluorescence from both large Au NPs (tens of nanometers) [47] and smaller metal clusters (<2 nm) [48] are ruled out. Third, this is not a comprehensive review but rather discusses key developments and applications, and we apologize for possible oversights of some significant contributions.

LSPR property of noble metal NPs

As early as 1857, Michael Faraday discovered that "fine particles" could be fabricated by treating aqueous chloroauric acid with phosphorus dissolved in carbon disulfide in a two-phase system [49]. The aqueous suspension of such "fine particles" displays a beautiful, ruby red color (Fig. 1b), which is completely different from the golden yellow color of their bulk counterpart. In 1908, Gustav Mie, a German physicist, well explained the optical phenomenon of the "fine particles" by solving the Maxwell equations: the intense red color of Faraday's samples can be attributed to the absorption and scattering of light by the Au NPs contained within the samples [50]. When light impinges on an Au (or Ag) NP, the free electrons of the metal will immediately sense the electromagnetic field and begin to oscillate collectively relative to the lattice of positive ions at the same frequency as the incident light. A schematic illustration in Fig. 1a shows this phenomenon for a metal nanosphere. This phenomenon is commonly known as LSPR, which can occur in any nanomaterial with an adequately high density of free charge carriers.

The LSPR behaviors of metal NPs are strongly dependent on their morphology. For metal nanospheres, the free electrons have only one kind of oscillation mode (up, Fig. 1a), and the oscillation frequency is less size-dependent according to the calculations of Mie theory [50]. As shown in Fig. 1c, the LSPR bands of spherical gold NPs always locate at about 520 nm as their size changes from 2.5 to 14 nm, whereas for non-spherical metal NPs, the situations are more complicated. For example, in the case of gold nanorods (AuNRs), one of the most studied non-spherical metal NPs, electron oscillation can occur in one of two directions depending on the polarization of incident light, namely, the short and long axes (down, Fig. 1a) [25]. The excitation of the oscillation along the short axis induces an absorption band in the short wavelength region, referred to as the transverse band. The excitation of the surface plasmon oscillation along the long axis induces a much stronger absorption band in the longer wavelength region, referred to as the longitudinal band. Furthermore, the transverse band locates at about 515–520 nm and is insensitive to the size of the NRs; in contrast, the longitudinal band is red-shifted largely from the visible to near-infrared region with increasing aspect ratio (Fig. 1d). The optical behaviors can be well understood according to Gans theory [51], which was developed for the explanation of optical properties of ellipsoid particles based on a dipole approximation. To other shaped NPs, such as, nanoplates, nanocubes, and nanocages, their oscillation often involves quadrupole and even higher poles, the LSPR bands are correspondingly more complicated. The readers can consult Refs. [27, 28, 30] for more information on the shape-dependent optical properties of metal NPs.

One- (or quasi-one) dimensional nanorod metal NPs

We herein use AuNRs as an example to demonstrate the sensing/biosensing applications of (quasi-) one-dimensional metal NPs, as considering that AuNRs are one of most famous non-spherical metal NPs. Owing to tunable optical properties and specific functions, AuNRs have been well studied from controllable synthesis to various potential applications. Based on seed mediated method, AuNRs have been well fabricated in the presence of 0.1 M cetyltrimethyl ammonium bromide (CTAB). Furthermore, the aspect ratio of the products can be modulated by the amounts of the added Ag^{+} ions [27]. To date, AuNRs have been widely used in photothermal therapy, molecular imaging, gene delivery, and data storage. Meanwhile, their sensing/biosensing applications have attracted increasing interest of analytical scientists. Based on the roles of AuNRs in the sensing/biosensing systems, the corresponding systems can be divided into several categories.

Colorimetric system

In 2005, Thomas and co-workers developed a simple colorimetric platform for cysteine and glutathione sensing using unmodified AuNRs as building blocks and reporters [52]. The side face of AuNRs synthesized by colloidal methods is densely capped by a double layer of CTAB molecules; in contrast, the two tips are less protected because of anisotropic property. As the analytes were introduced into the AuNR solution, the thiols bound onto the Au rod tips by Au-S conjunction, and the terminated amino and carboxyl groups at different rods attracted each other by two-point electrostatic interaction. As a result, end-to-end (EE) self-assembly of the AuNRs was observed, which accompanied a ratiometric signal readout. The sensitivity could reach to micromolar concentration level. Other amino acids did not cause the AuNR assembly because of lack of the corresponding functional groups. The sensing processes were performed in acetonitrile/water (4:1) medium. Obviously, it was less biocompatible. Then, this system was improved and extended to complete aqueous medium by Wang group [53], which correspondingly enhanced its application potential.

Subsequently, Wang et al. successfully assayed microcystin-LR (MC-LR), one of the pervasive environmental toxins, using MC-LR antibodies-modified Au nanorods as reporters [54]. By rationally modifying sides or ends of Au nanorods, side-by-side (SS) or EE assembly was achieved, respectively (Fig. 2a and b). Both of the assembly modes could be employed for the detection of MC-LR, and EE mode was more sensitive than that of SS (0.03 versus 0.6 ng mL^{-1}) (Fig. 2c). The sensing parameters for MC-LR using the AuNR assemblies surpassed the required standard of drinking water by the World Health Organization (1 μg L^{-1}), indicating their potential applications. In addition, based on versatile chemical modification and various recognition principles, AuNR assembly system was also used for the detection of Hg^{2+} [55, 56], amino acids [57], proteins [58, 59], etc.

Recently, Lu and Xia presented enzymatic reaction-modulated self-assembly of AuNRs; furthermore, it was applied in colorimetric assays of cholinesterase (ChE) and organophosphate pesticides (OPs) in human blood [60]. The sensing processes are shown in Fig. 3a: in the absence of ChE, cysteine molecules selectively bind to the tips of AuNRs based on S−Au conjunction, which causes the AuNR EE assembly and form well-defined one-dimensional architectures [52]. As ChE is introduced, pre-added substrate (acetylthiocholine) is catalyzed and decomposed to thiocholine and acetate acid. The resulting thiols can also bind to the tips of the AuNRs and effectively prevent the subsequent cysteine-induced self-assembly (Fig. 3b). As a result, the AuNR LSPR band is modulated and a distinctly ratiometric signal output is obtained (Fig. 3d). The linear range is 0.042 to 8.4 μU/mL and the detection limit is as low as 0.018 μU/mL. As ChE is incubated with OPs, the enzymatic activity is effectively inhibited. So, the cysteine-induced AuNR EE assembly is observed again (Fig. 3e). On the basis of this principle, OPs are well determined ranging from 0.12 to 40 pM with 0.039 pM detection limit. As far as we know, the present quasi-pU/mL level sensitivity for ChE and quasi-femtomolar level sensitivity for OPs are at least 500 and 7000 times lower than those of previous colorimetric methods, respectively. In the present system, the ultra-high sensitivity can be attributed to two reasons. The first is the rational choice of anisotropic AuNRs as building blocks and reporters. The used AuNRs have rather inert side face, and only the two tips are active for the interactions with thiocholine/cysteine molecules. This "enriching" effect well enhances the dispersion/assembly modulation effect, compared with homogenously surfaced Au nanospheres. The second is the specific structure of the enzymatic thiocholine. The appended thiocholine molecules, on the one hand, occupy cysteines' binding sites; on the other hand, increase the electrostatic repulsion among the AuNRs because of their strongly positively charged quaternary ammonium groups. Such dual effect substantially inhibits the cysteine-induced self-assembly. Owing to ultrahigh sensitivity, serum samples are allowed to be extremely diluted for the assay. So, various nonspecific interactions, even from glutathione/cysteine, can be well avoided (Fig. 3c). Accordingly, both ChE and OPs in human blood can be directly assayed without any sample pre-purification processes, indicating the simplicity and practical promise of the proposed system. The study of enzymatic reaction-modulated AuNR assembly is important. Conceivably, in combination with enzyme-linked immunosorbent assay (ELISA), versatile and powerful assay platforms can be constructed for various bio-assay applications.

It is known that the LSPR band of metal NPs is sensitive to dielectric environment. According to this theory, AuNR-based

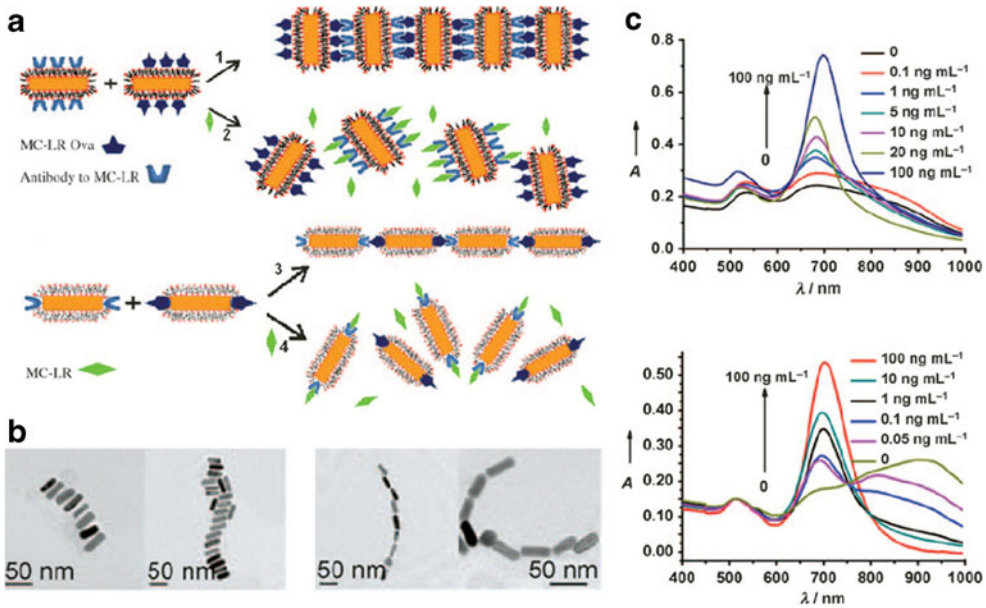

Fig. 2 Colorimetric assay of MC-LR by the analytes-induced AuNR assembly. (**a**) Schematic illustration of toxin detection system based on SS (above) and EE (below) NR assemblies. (**b**) Representative TEM images for SS and EE NR assemblies. (**c**) Evolution of LSPR spectra of the NRs upon increasing concentrations of MC-LR indicated in the graph for side-to-side (above) and end-to-end (below) assemblies; Figure reprinted with permission from Ref. [54]

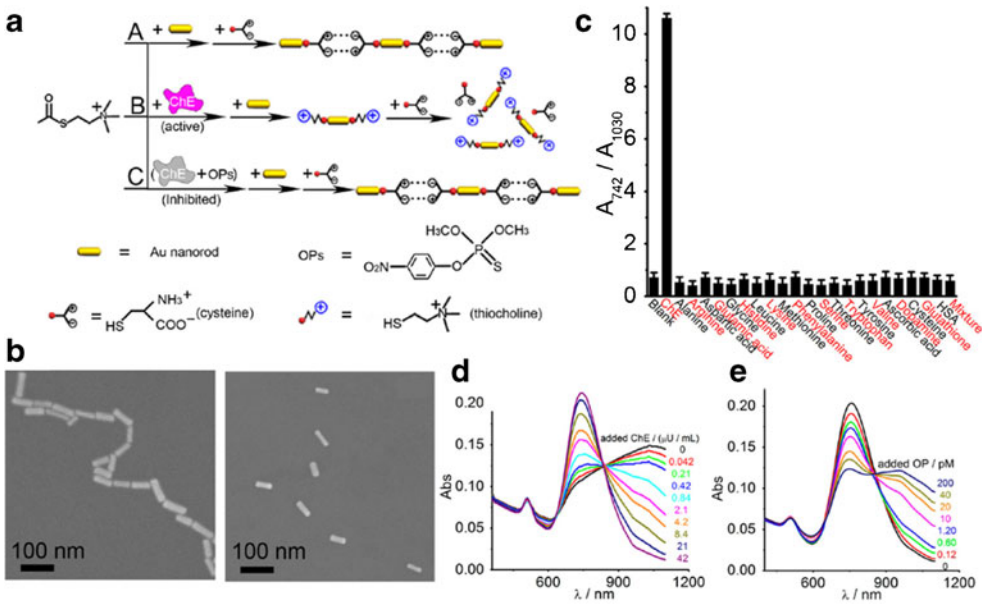

Fig. 3 Enzymatic reaction-modulated AuNR self-assembly for sensing of ChE and OPs. (**a**) Schematic illustration of the assay platform. (**b**) (acetylthiocholine + AuNRs + cysteine) system (left), and (acetylthiocholine + ChE + AuNRs + cysteine) system (right). (**c**) Assay system toward various potential interfering substances. (**d**) Absorbance response of the AuNR-based assay system to ChE. (**e**) Absorbance response of the AuNR-based assay system to parathion; Figure reprinted with permission from Ref. [60]

sensing/biosensing systems for various analyte targets were constructed. For example, Yu and Irudayaraj fabricated antibody-modified AuNRs and employed them for assay of antigens [61]. As the targets bind onto the AuNRs, the refractive index in the vicinity of the AuNRs is changed, which causes the red shift of the longitudinal bands about 20–30 nm. The system could assay three antigen targets simultaneously by using three kinds of AuNRs with different binding sites and aspect ratios. Based on targets-induced change in local refractive index, a chip-based, label-free plasmonic biosensor was fabricated for the detection of model analytes (streptavidin) in serum, using AuNRs as reporters [62]. This assay strategy was further extended to single AuNR detection, and the detection of streptavidin could be low to 1 nM [63]. In addition to biomacromolecules, such signal transduction strategy was also employed for inorganic ion sensing. With the assistance of $Na_2S_2O_3$, $NaBH_4$, and $HgCl_2$, Cu^{2+} ions could cause a shell around the AuNRs, which led to a red shift of the longitudinal band of the host AuNRs. Based on this reaction, Cu^{2+} ions were successfully assayed in different bio-samples, including human serum, human urine, and red blood cells [64].

Furthermore, the LSPR of AuNRs, especially for longitudinal band, is extremely sensitive to their aspect ratio. Campiglia group found that Hg^{2+} ions could etch AuNRs assisted by $NaBH_4$, based on the amalgamation of Hg with Au. As a result, the aspect ratio of the AuNRs decreased and a blue shift of the longitudinal band was observed. The proposed method possessed high sensitivity (6.6×10^{-13} g L^{-1}) and could sense trace of Hg^{2+} ions in tap water [65]. By means of etch reactions, AuNR-based systems were also employed in the assay of glucose [66], Co^{2+} [67], molybdate [68], nitrite [69], etc.

Fluorescent system

Because of versatile surface modification, tunable LSPR band, as well as high extinction coefficient, AuNRs should be a favorable energy acceptor for the design of the FRET sensing platform [70]. For example, Zhu and co-workers constructed a FRET system for assay of human immunoglobulin G using AuNR and QDs as receptors and donors, respectively [71]. In their system, the energy transfer efficiency is only 9 %, although the optical bands of the two particles are well overlapped. Such low efficiency limited the analytical performances and applications. The probable reason for the low FRET efficiency was the long distance between the donors and the receptors, considering that the used AuNRs were capped by a double layer of CTAB molecules with 3–5 nm thickness. To solve this problem, Xia et al. employed short thiols, namely cysteamine, to replace the CTAB molecules. The resulting amine-terminated AuNRs could interact with mercaptopropionic acid-modified QDs and form compactly hybrid (AuNR-QDs) assembly (Fig. 4a). As a result, the QD emission was quenched more than 90 %, which almost completely eliminated the background fluorescence of the QDs. Trinitrotoluene (TNT), one of the highly explosives and environmentally detrimental substances, could react with amino group around the AuNRs and form Meisenheimer complexes, leading to the replacement of the attached QDs and a dramatic fluorescence recovery of the QDs (Fig. 4b). As a result, TNT was determined ranging from 0 to 66 nM by turn-on signal readout, and the detection limit was as low as 0.1 nM (Fig. 4c) [72].

Recently, Wong and co-workers designed a Au NP-locked nucleic acid (LNA) biosensor for spatiotemporal mapping mRNA gene expression in both living cells and tissues [73].

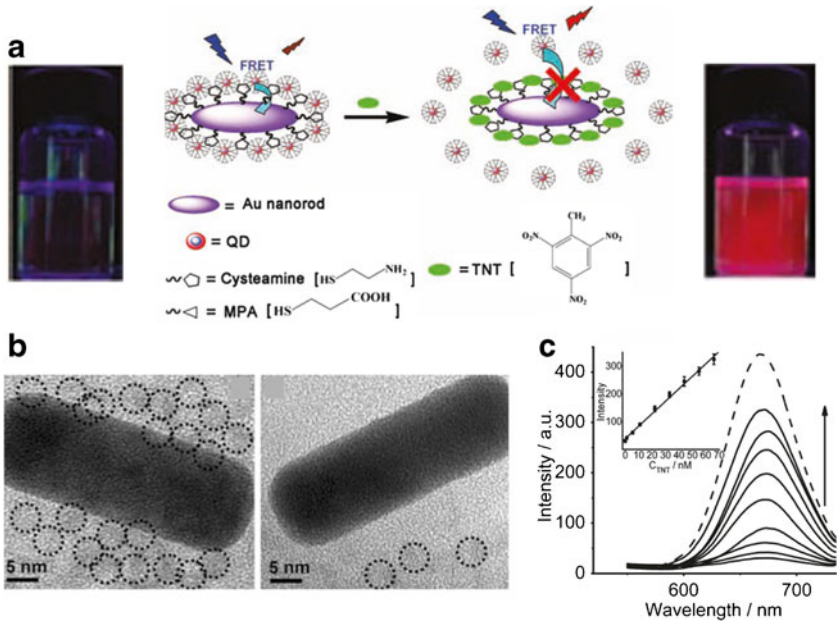

Fig. 4 Turn-on and near-infrared sensing of TNT by AuNR-QDs assembly. (**a**) The sensing schematic illustration. (**b**) TEM images of the hybrid AuNR-QDs assembly before (left) and after (right) addition of TNT molecules. (**c**) Evolution of emission spectra of AuNR-QDs assemblies with increasing TNT, the corresponding linear plots are shown in the inset; Figure reprinted with permission from Ref. [72]

The work scheme is shown in Fig. 5a: First, the fluorophore-labeled LNA binds spontaneously to the Au NPs and forms NP-LNA complexes; because of the affinity of LNA and gold NPs, the fluorophore is correspondingly quenched by FRET effect. Second, in the presence of the target mRNA, the labeled LNA is thermodynamically displaced from the Au NPs and binds to the specific mRNA target sequence because of their higher binding affinity. The binding reaction makes the LNA probe leave the Au surface and recovers the emission of the quenched fluorophores. The concentration of the target mRNA can, therefore, be determined dynamically based on the fluorescence intensity, even in each individual cell. The nonspecific interactions are rather low (Fig. 5d). Interestingly, the authors found that an AuNR-based sensing system possesses higher signal-to-noise ratio than that of spherical Au NP-based one (Fig. 5c). The proposed AuNR-LNA probes possess several distinct advantages. First, mRNA expression can be detected in complex cell structures at single cell level, which is critical to study the emergency and heterogeneity in complex biological processes. Then, the probe is excellently stable and low toxic, which can work for dynamic gene expression analysis in living cells analysis over 24 h. Third, the technique can be implemented by only an incubation step; any transfection and injection are needless. So, it well decreases the perturbation of the assayed cells. Furthermore, this technique can be easily

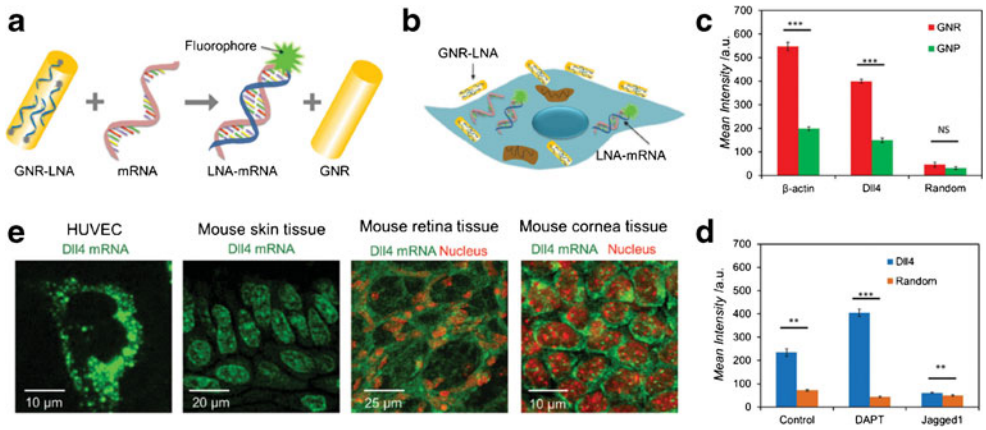

Fig. 5 AuNR-LNA for single cell gene expression analysis in living cells and tissues. (**a**) Schematic of the AuNR-LNA biosensor. (**b**) Endocytic uptake of the AuNR-LNA probe by cells for intracellular detection. (**c**) Mean fluorescence intensities of β-actin, Dll4, and random probes in HUVEC. (**d**) Mean fluorescence intensities of random and Dll4 probes under different treatments. (**e**) Dll4 mRNA gene expression (green) in HUVEC, mouse skin, retina, and cornea tissues. For mice retina and cornea tissues, the nuclei of epithelial cells were stained using TO-PRO-3, cytoplasm of epithelium cells were recognized by Dll4probe. Images are representative of three independent experiments; Figure reprinted with permission from Ref. [73]

adapted to detect different genes and is applicable in various types of cells and tissues, including primary cells and intact animal tissues (Fig. 5e).

In addition to QDs and organic dyes, the fluorescent donors could also be served by rare earth element-doped NPs [74]. So far, the FRET systems made of AuNRs and various fluorophores have been exquisitely designed and applied for sensing of various analyte targets, including inorganic ions [75, 76], DNA [77], virus antigens [78], etc. based on either turn-off or turn-on signal output.

Two-dimensional nanoplate metal NPs

In 2001, Mirkin and co-workers found that Ag nanospheres could convert into nanoprisms by fluorescent light illumination [79]. Subsequently the synthesis of metal nanoplates has been well explored. Now, both Ag [80] and Au [81] nanoplates can be reproducibly fabricated by more facile and time-saving approaches. In addition to high purity, the thickness and length of the products could also be controlled by sophisticated chemistry. These achievements are significant to the study of their properties and applications. Because of reliable synthesis method and favorable optical property, Ag triangular nanoplates, named nanoprisms, were chosen as examples to demonstrate the sensing/biosensing of two-dimensional noble metal NPs.

Colorimetric system

The LSPR band of Ag nanoplates is very sensitive to their shape. So, based on the shape modulation of analyte targets, various sensing/biosensing systems could be constructed. In 2009, Huang and co-workers developed a simple system for sensing of cysteine by the analyte-etched Ag nanoprisms [82]. In the presence of cysteine, Ag nanoprisms turned into discs because of S–Ag interactions. Accordingly, the LSPR bands of the Ag nanoplates shift to blue region. Other amino acids, because of lack of thiols, could not induce the shape changes of the Ag nanoprisms. Such system provided a potential for visualized assay of cysteine. Then, Chen et al. employed 1-dodecanethiol-modified Ag nanoprisms for sensing of Hg^{2+} ions [83]. Because of strong affinity between Hg^{2+} ions and thiols, 1-dodecanethiol molecules were stripped from the Ag nanoprism surface by the added Hg^{2+}. Then, the de-protected nanoprisms were etched to nanodiscs by iodide ions, resulting in a change of the solution color and absorption spectra. The method could determine Hg^{2+} ranging from 10 to 500 nM with 3.3 nM detection limit. Such etch strategy could also be achieved in substrate. Recently, Chen and co-workers developed a sensor consisting of Ag nanoprisms anchored on a glass substrate and an overlayer of polyelectrolyte thin film on top of the NPs [84]. The analyte-sensitive DNA aptamers were put in the film in advance by the layer-by-layer technique, which acted as a "biological gate" to control the diffusion of a chemical etchant. The binding between the analytes and the aptamers opened up the pores in the film and facilitated the permeation of the etchant (I^-/I_3^-). Thus, the Ag nanoprisms were well etched and a LSPR shift was observed. Because the structure and recognition capability of DNA aptamers can be well designed, such concept provided the basis for potentially low-cost, portable, chip-based colorimetric sensors.

The shape and size change of Ag nanoprisms could also be achieved by enzymatic reaction. Xia and co-workers developed a system consisting of Ag nanoprisms and glucose oxidase (GOx) for sensing of glucose in human blood (Fig. 6a) [32]. In the presence of the analytes, the enzymatic H_2O_2 etch the triangular Ag nanoprisms into smaller nanodiscs (Fig. 6b) accompanied by a more than 100 nm blue shift of the LSPR peak. The detection limit was as low as 0.2 μM. Owing to high sensitivity, most of the various interferences from biomatrix could be well avoided by substantial dilution in blood sugar assay (above of Fig. 6c). The only remaining interfering substance was uric acid, which could strongly bind onto the sides (110 facets) of the Ag nanoprisms and prevent the etch reaction [34]. Fortunately, such interference could be eliminated by the coordination reaction between uric acid and Fe^{2+} (below of Fig. 6c).

In addition to blood sugar assay, such enzymatic reaction-modulated shape and size change of Ag nanoprisms is a favorable signal output system. For example, by combination of this system and hybridization chain reaction, Gao and co-workers performed DNA assay, and the detection limit decreased to 6 fM [85]. If associated with immunoreactions (namely, ELISA technique), it could also be employed for antigen assay, as demonstrated by the Tang group [86].

Fluorescent system

Recently, Wang and co-workers developed a (conjugated polymer-Ag nanoprism) system for label-free biomarker assay based on the analytes-modulated plasmon-enhanced fluorescence (PEF) (Fig. 7) [87]. The assay system was fabricated as follows: quartz slides that adsorbed Ag nanoprisms acted as metal magnifying nanostructures. The obtained metal substrate was then covered by interlayer film composed of polyethyleneimine/poly-(acrylic acid) (PAA) pair. After antibody bioconjugation with carboxylic acid group of PAA, the antibody–antigen recognition can adopt a distance variation between surface bound conjugated polymer (poly [9,9′-bis(6,6′-(N,N,N-trimethylaminium)fluorene-2,7-ylenevinylene-co-alt-2,5-dicyano-1,4-phenylene], PFVCN) and bottom Ag nanostructure to tune the PEF effect, and further to realize a change in fluorescent signal of PFVCN. As shown in Fig. 7a and b, in the absence of the targets, the added

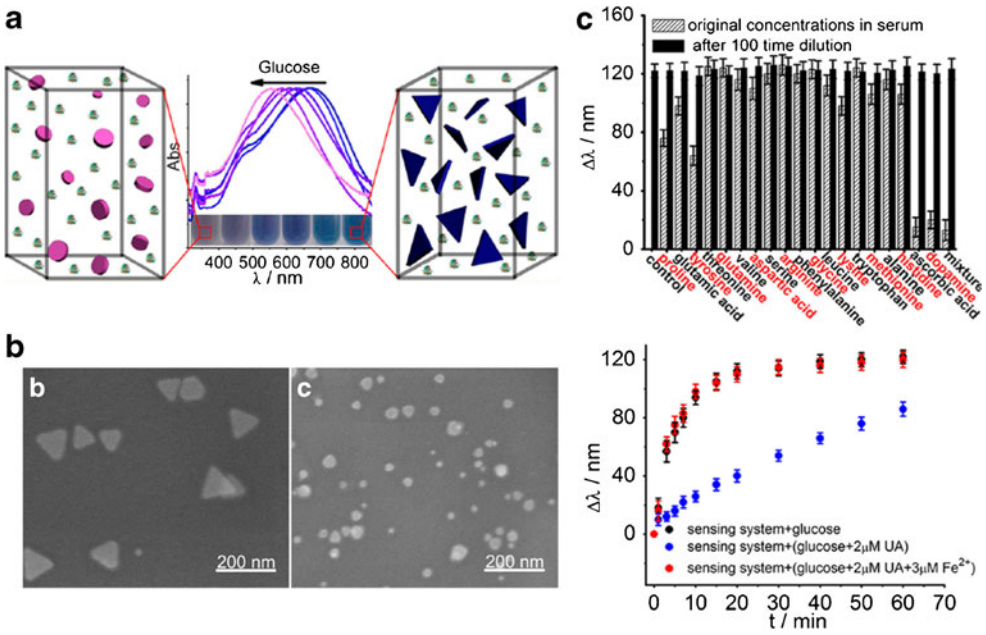

Fig. 6 Sensing of glucose by Ag nanoprisms-GOx system. (**a**) The sensing schematic illustration. (**b**) TEM images of the sensing system in the absence (left) and presence (right) of glucose. (**c**) The sensing system toward various potential interfering substances; Figure reprinted with permission from Ref. [32]

PFVCN molecules directly interacted with the antibody layer. Meanwhile, a strong PEF effect was observed. In contrast, in the presence of the targets [antiprostate-specific antigen (PSA)], the distance between the fluorescent molecules and the Ag nanoprisms was enhanced by the antibody–antigen reaction, which caused the decrease of the PEF effect. As a result, a weaker fluorescence was obtained. Based on the distance-dependent PEF modulation, the detection limit for PSA was 9.7 μg mL^{-1}. Furthermore, the system possessed various highly selective proteins and did not interfere with the assay (Fig. 7c) In addition to free antigens, the proposed system could also detect membrane antigens and recognize the designed cancer cells (Fig. 7d), indicating its clinical sensing application potentials.

As described above, Ag nanoplates possess high extinction coefficient and widely tunable LSPR band, which can well modulate the fluorescent behaviors of fluorophores in the vicinity of the metal NPs. Interestingly, in addition to fluorescence modulation, Ag nanoprisms could also enhance analytical performance. Batteas and co-workers fabricated a

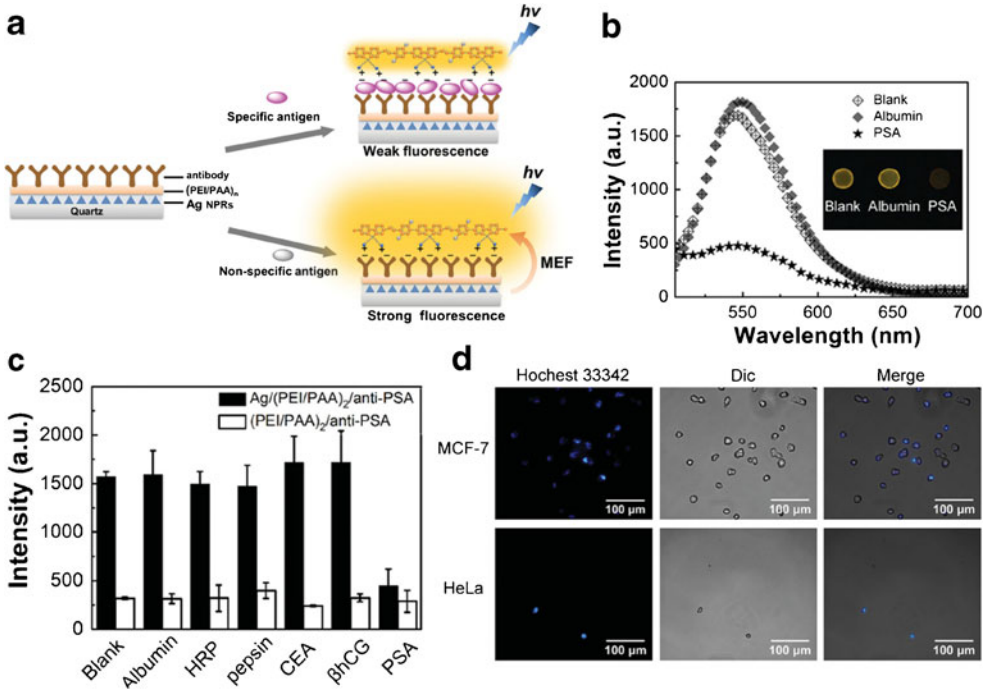

Fig. 7 Ag nanoprism-based PEF system for sensing of PSA. (**a**) Schematic illustration of the sensing system. (**b**) Emission spectra of PFVCN before and after incubation with albumin and PSA. Inset: fluorescence photographs of PFVCN before and after incubation with albumin and PSA. (**c**) Intensity of PFVCN on Ag/$(PEI/PAA)_2$/anti-PSA and $(PEI/PAA)_2$/anti-PSA platform after incubation with different proteins. (**d**) Microscopy images of nuclear stained MCF-7 (positive cell) and HeLa cell (negative cell) capturing on Ag/$(PEI/PAA)_2$/anti-EpCAM film; Figure reprinted with permission from Ref. [87]

self-assembled film consisting of Ag nanoprisms and CdSe QDs for fluorescent sensing of Cu^{2+} ions [88]. The film was deposited on Si substrate made of Ag nanoprisms, polymers and CdSe QDs. The polymer layer, between the Ag and CdSe, was used to space the metal NPs and QDs with an optimal separation distance. So, the QD fluorescence was enhanced by the strong electric field of the Ag nanoprims, instead of quenching effect by FRET effect. Cu^{2+} ions could quench the CdSe QDs fluorescence based on the cation exchange of Cu^{2+} and Cd^{2+} on the QD surface. The quenching effect could be enhanced as the CdSe QDs had been photo-brightened by light irradiation. In the presence of Ag nanoprisms, the sensitivity for Cu^{2+} detection was further enhanced; furthermore, the dynamic range was dramatically increased regardless of whether the QDs were photo-brightened or not.

Three-dimensional nanodendritic metal NPs

In this review, nanodendritic NPs refer to metal NPs with superstructures at three-dimensional space, which also are named as nanostars or nanoflowers by a few authors. Because of strongly electromagnetic enhancement effects (antenna effect + hot spots), Au and Ag nanodendritic NPs have been well employed as the substrates for SERS applications. Recently, this type of NPs have also been used as reporters and emission modulators for the design of ultra-sensitive colorimetric and fluorescent sensing systems, respectively.

Colorimetric system

For Au NDs, the high-aspect-ratio spikes can well localize the low-energy plasmon mode at their tips, which results in a dominant LSPR band in near-infrared region. As a result, Au NDs are one of the favorable candidates for signal readout in bio-assay.

The Stevens groups constructed an Au ND-based ELISA system for PSA assay, which possessed an interestingly counterintuitive inverse sensitivity enabled by enzyme-guided crystal growth [89]. The assay principle is shown in Fig. 8a: the LSPR band is tuned by programming crystal growth to favor either the formation of a silver coating around the transducer or the nucleation of silver nanocrystals in solution. To control crystal growth, they used GOx, which generates hydrogen peroxide that reduces silver ions around the Au NDs. When the enzyme is present at low concentrations, the short supply of reducing agent dictates slow crystal growth conditions. This favors the growth of a homogeneous silver coating on the Au ND as seeding points (left of Fig. 8b), which yields a blue-shift in the LSPR of the nanosensors. However, when the concentration of GOx is high, the abundant reducing agent favors nucleation instead of epitaxial growth, and free-

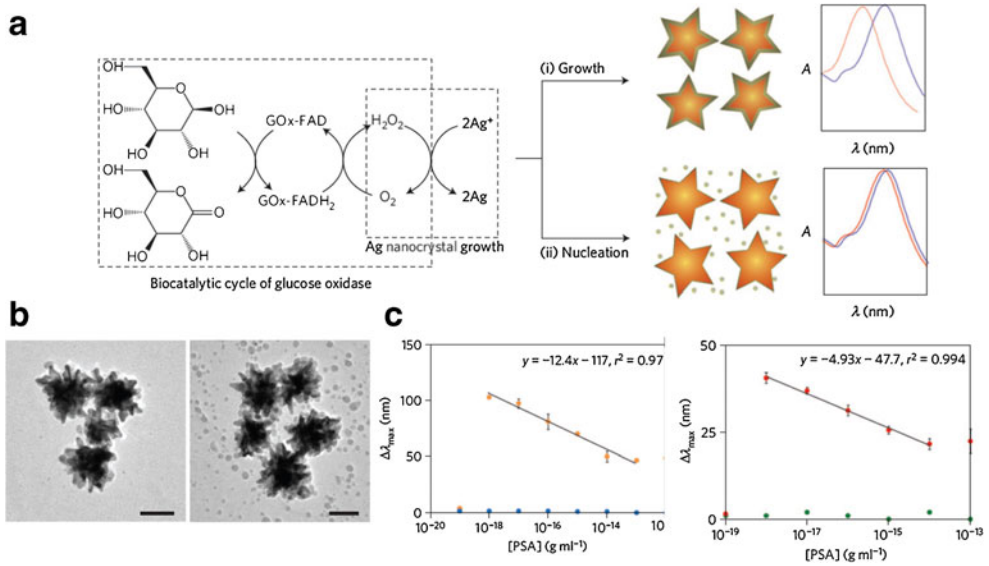

Fig. 8 Au ND-based ELISA system for PSA assay with counterintuitive inverse sensitivity. (**a**) Scheme of the proposed signal-generation mechanism by means of enzyme-guided crystal growth. GOx generates hydrogen peroxide, which reduces silver ions to grow a silver coating around plasmonic nanosensors (gold nanostars); (i) at low concentrations of GOx the nucleation rate is slow, which favors the growth of a conformal silver coating that induces a large blueshift in the LSPR of the nanosensors; (ii) when GOx is present at high concentrations, the fast crystal growth conditions stimulate the nucleation of silver nanocrystals and less silver is deposited on the nanosensors, therefore generating a smaller variation of the LSPR. When the concentration of GOx is related to the concentration of a target molecule through immunoassay, this signal-generation step induces inverse sensitivity because condition (i) is fulfilled at low concentrations of analyte. (**b**) TEM pictures after the signal-generation step when gold nanostars were modified with 10^{-20} g mL^{-1} GOx (left) and 10^{-14} g mL^{-1} GOx (right). (**c**) Blueshift of the LSPR absorbance band as a function of the concentration of PSA (orange) and BSA (blue) in PBS (left) and of PSA (red) and BSA (green) spiked into whole serum (right); Figure reprinted with permission from Ref. [89]

standing silver NPs are obtained (right of Fig. 8b). Consequently, less silver is deposited on the nanosensors and the LSPR shifts less than in the presence of GOx at low concentrations. By combination of such enzyme-modulated dynamics nucleation or growth and immunoassay, the proposed system was employed for the assay PSA. As shown in Fig. 8c, the nanosensors could well assay the antigen in both PBS buffer solution and whole serum, and the sensitivity was as high as 4×10^{-20} M in both systems.

Fluorescent system

Chen and Xia present a PEF system for label-free sensing of small organic dyes in bulk solution based on hybrid (AuND-QDs) assemblies (Fig. 9a) [90]. The amine-terminated Au NDs and carboxyl-terminated QDs directly assemble each other by amine−carboxyl attraction. Without any spacer layers, PEF can be increased by four times during the formation of the compact hybrid (AuND-QDs) assembly (Fig. 9c). The remarkable PEF effect could arise for two reasons: (1) the used AuNDs simultaneously possess four features in morphology and topology, well-defined superstructure, sharp tips and edges, moderately elongated subunits, and smaller size; (2) the hybrid (AuND-QDs) assembly has a very compact structure. So, the fluorescence is well enhanced by the effective increase of excitation and radiative decay rates by the strong electric field (Fig. 9b) with the decrease of scattering effect. The (AuND-QDs) assembly is then employed for sensing of TNT in bulk solution. The sensing principle is that the analytes can react with primary amines on the AuND surface and form Meisenheimer complexes [72], which break the preformed assemblies and result in the fluorescence recovery of the QDs. The linear range is 0−8.8 nM with 0.05 nM detection limit (Fig. 9d). The present quasi-picomole level sensitivity is one of the best results for fluorescent TNT sensing. The developed method is successfully applied to TNT sensing in real environmental samples, indicating the practical potential. The traditional PEF systems often employed bulky (several hundred nanometers) NPs, which cannot work in solution because (1) they are not stable in solution because of gravitational effect, and (2) they strongly scatter the enhanced emission and lead to fluorescence quenching. So, previous PEF assay systems only performed on substrates, and the analyte targets were often limited to DNA and proteins assisted by labeling technique. In the present system, based on the rational choice of AuNDs as emission modulator, label-free sensing in bulk solution was achieved.

Metal NPs with other morphology

In addition, metal NPs metal nanowire [91], nanocages [92], and even asymmetric janus particles [93] have also been fabricated by sophisticated synthetic techniques. In addition to shape-regulated optical properties, a few NPs with special morphology, such as hollow structure, possess multifunctional potential applications. For example, the Qu group developed a theranostic nanomedicine combined by pH sensitive fluorophores and gold nanocage, which can be employed for the simultaneous detection and treatment of cancer [94].

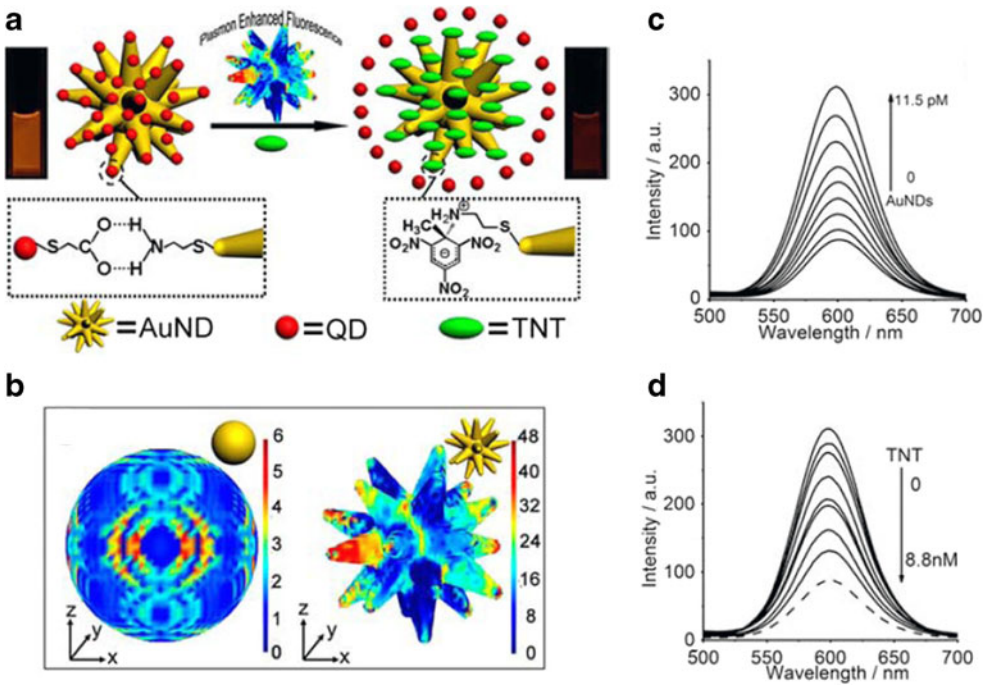

Fig. 9 PEF system for sensing of TNT in solution by hybrid (AuND-QDs) assemblies. (**a**) Schematic illustration of the system. (**b**) The distribution of surface electric field simulated with single Au nanosphere and AuND. (**c**) Evolution of fluorescence spectra of QDs with increasing AuNDs concentrations. (**d**) Evolutions of emission spectra of the hybrid (AuND-QDs) assemblies with increasing TNT, the concentrations of which from top to bottom are 0, 0.88, 2.2, 4.0, 5.5, 6.6, 7.7, and 8.8 nM, respectively; Figure reprinted with permission from Ref. [90]

Concluding remarks and prospects

Although considerable progresses in the study of non-spherical metal NP-based sensing/biosensing have been made in recent years, there still are several significant issues deserving in-depth exploration. Further systematic research both in experiments and theories is needed for fundamental understanding and better applications of non-spherical NPs.

First, for rational design (metal NPs-fluorophores)-based sensing systems, intensive study should be diected to the effects of metal NPs on the fluorescence modulation of the vicinity fluorophores. There are at least three kinds of mechanism on metal−fluorophore interactions [95]; furthermore, lots of factors, such as size/shape of metal NPs, fluorescence quantum yield of fluorophores, the distance of metal NPs and fluorophores, etc. can profoundly affect their interactions. So, in addition to comprehensive experiments, theoretical calculations should also be essential for interpreting such fundamental photophysical processes.

Second, the development of novel sensing systems based on new signal transduction is extremely significant. For example, Tang and co-workers proposed an Au NR assembly system for DNA assay using circular dichroism (CD) as signal readout [96]. Because of strong coupling LSPR of Au NRs and the chiral signal of DNA molecules, the plasmon CD responses were much more sensitive than those of absorption spectra. The detection limit is as low as 75 nM. So, the exploration of new signal transduction modes beyond the traditional ones (fluorescence, absorption, Raman scattering) is promising for expanding the applications and/or enhancing the analytical performances of metal NP-based sensing/biosensing platform.

Third, multiple-readout sensing/biosensing systems are desirable. Up to now, most of the studied sensing/biosensing systems were based on single signal output. Conceivably, the analytical performances, especially for reliability, would be substantially improved if multiple signals are employed (for example, LSPR + fluorescence, LSPR + dynamic light scattering, LSPR + SERS, etc.) in sensing/biosensing. In fact, a few assay systems with multiple-signal-readout have been reported [97], and some of them exhibited better performances. Because non-spherical metal NPs possess widely tunable LSPR bands and specific facet-dependent physicochemical (catalysis, adsorption, electromagnetic enhancement, etc.) properties, they should have great potentials in the design of multiple signal readout for sensing/biosensing systems.

Acknowledgments This work is financially supported by the National Natural Science Foundation of China (nos. 21275001 and 21422501).

Compliance with ethical standards

Conflict of interest The author declares no conflict interest.

References

1. Medintz IL, Uyeda HT, Goldman ER, Mattoussi H (2005) Quantum dot bioconjugates for imaging, labeling and sensing. Nat Mater 4(6):435–446
2. Freeman R, Willner I (2012) Optical molecular sensing with semiconductor quantum dots (QDs). Chem Soc Rev 41(10):4067–4085
3. Wu P, Hou X, Xu JJ, Chen HY (2014) Electrochemically generated versus photoexcited luminescence from semiconductor nanomaterials: bridging the valley between two worlds. Chem Rev 114(21):11027–11059
4. Vannoy CH, Tavares AJ, Noor MO, Uddayasankar U, Krull UJ (2011) Biosensing with quantum dots: a microfluidic approach. Sensors 11(12):9732–9763
5. Liu Z, Tabakman S, Welsher K, Dai H (2009) Carbon nanotubes in biology and medicine: in vitro and in vivo detection, Imaging and drug delivery. Nano Res 2(2):85–120
6. Wang J (2005) Carbon-nanotube-based electrochemical biosensors: a review. Electroanalysis 17(1):7–14
7. Chang J, Zhou G, Christensen ER, Heideman R, Chen J (2014) Graphene-based sensors for detection of heavy metals in water: a review. Anal Bioanal Chem 406(16):3957–3975
8. Shao Y, Wang J, Wu H, Liu J, Aksay IA, Lin Y (2010) Graphene-based electrochemical sensors and biosensors: a review. Electroanalysis 22(10):1027–1036
9. Yavari F, Koratkar N (2012) Graphene-based chemical sensors. J Phys Chem Lett 3(13):1746–1753
10. Na HB, Song IC, Hyeon T (2009) Inorganic nanoparticles for MRI contrast agents. Adv Mater 21(21):2133–2148
11. Gao J, Gu H, Xu B (2009) Multifunctional magnetic nanoparticles: design, synthesis, and biomedical applications. Acc Chem Res 42(8):1097–1107
12. Li YC, Lin YS, Tsai PJ, Chen CT, Chen WY, Chen YC (2007) Nitrilotriacetic acid-coated magnetic nanoparticles as affinity probes for enrichment of histidine-tagged proteins and phosphorylated peptides. Anal Chem 79(19):7519–7525
13. Saha K, Agasti SS, Kim C, Li X, Rotello VM (2012) Gold nanoparticles in chemical and biological sensing. Chem Rev 112(5):2739–2779
14. Wilson R (2008) The use of gold nanoparticles in diagnostics and detection. Chem Soc Rev 37(9):2028–2045
15. Daniel MC, Astruc D (2004) Gold nanoparticles: assembly, supramolecular chemistry, quantum-size-related properties, and applications toward biology, catalysis, and nanotechnology. Chem Rev 104(1):293–346
16. Li H, Rothberg L (2004) Colorimetric detection of DNA sequences based on electrostatic interactions with unmodified gold nanoparticles. Proc Natl Acad Sci U S A 101(39):14036–14039
17. Jain PK, Huang X, El-Sayed IH, El-Sayed MA (2008) Noble metals on the nanoscale: optical and photothermal properties and some applications in imaging, sensing, biology, and medicine. Acc Chem Res 41(12):1578–1586
18. Guo L, Jackman JA, Yang HH, Chen P, Cho NJ, Kim DH (2015) Strategies for enhancing the sensitivity of plasmonic nanosensors. Nano Today 10(2):213–239
19. Zhou W, Gao X, Liu D, Chen X (2015) Gold nanoparticles for in vitro diagnostics. Chem Rev 115(19):10575–10636
20. Yang X, Yang M, Pang B, Vara M, Xia Y (2015) Gold nanomaterials at work in biomedicine. Chem Rev 115(19):10410–10488
21. Xu L, Kuang H, Wang L, Xu C (2011) Gold nanorod ensembles as artificial molecules for applications in sensors. J Mater Chem 21(42):16759–16782

22. Mirkin CA, Letsinger RL, Mucic RC, Storhoff JJ (1996) A DNA-based method for rationally assembling nanoparticles into macroscopic materials. Nature 382(6592):607–609
23. Elghanian R, Storhoff JJ, Mucic RC, Letsinger RL, Mirkin CA (1997) Selective colorimetric detection of polynucleotides based on the distance-dependent optical properties of gold nanoparticles. Science 277(5329):1078–1081
24. Dabbousi BO, Rodriguez-Viejo J, Mikulec FV, Heine JR, Mattoussi H, Ober R, Jensen KF, Bawendi MG (1997) (CdSe)ZnS core−shell quantum dots: synthesis and characterization of a size series of highly luminescent nanocrystallites. J Phys Chem B 101(46): 9463–9475
25. Yasun E, Kang H, Erdal H, Cansiz S, Ocsoy I, Huang YF, Tan W (2013) Cancer cell sensing and therapy using affinity tag-conjugated gold nanorods. Interface Focus 3:20130006
26. Zhang J, Tang Y, Lee K, Ouyang M (2010) Tailoring light–matter–spin interactions in colloidal hetero-nanostructures. Nature 406 (7302):91–95
27. Huang X, Neretina S, El-Sayed MA (2009) Gold nanorods: from synthesis and properties to biological and biomedical applications. Adv Mater 21(48):4880–4910
28. Sau TK, Rogach AL, Jäckel F, Klar TA, Feldmann J (2010) Properties and applications of colloidal nonspherical noble metal nanoparticles. Adv Mater 22(16):1805–1825
29. Orendorff CJ, Murphy CJ (2006) Quantitation of metal content in the silver-assisted growth of gold nanorods. J Phys Chem B 110(9): 3990–3994
30. Murphy CJ, Gole AM, Hunyadi SE, Stone JW, Sisco P, Alkilany A, Hankins PL, Kinard B (2008) Chemical sensing and imaging with metallic nanorods. Chem Commun 5:544–557
31. Liu X, Atwater M, Wang J, Huo Q (2007) Extinction coefficient of gold nanoparticles with different sizes and different capping ligands. Colloids Surf B: Biointerfaces 58(1):3–7
32. Xia Y, Ye J, Tan K, Wang J, Yang G (2013) Colorimetric visualization of glucose at the submicromole level in serum by a homogenous silver nanoprism−glucose oxidase system. Anal Chem 85 (13):6241–6247
33. Millstone JE, Wei W, Jones MR, Yoo H, Mirkin CA (2008) Iodide ions control seed-mediated growth of anisotropic gold nanoparticles. Nano Lett 8(8):2526–2529
34. Tan K, Yang G, Chen H, Shen P, Huang Y, Xia Y (2014) Facet dependent binding and etching: ultra-sensitive colorimetric visualization of blood uric acid by unmodified silver nanoprisms. Biosens Bioelectron 59:227–232
35. Jana NR, Pal T (2007) Anisotropic metal nanoparticles for use as surface-enhanced Raman substrates. Adv Mater 19(13):1761–1765
36. Aslan K, Lakowicz JR, Geddes CD (2005) Metal-enhanced fluorescence using anisotropic silver nanostructures: critical progress to date. Anal Bioanal Chem 382(4):926–933
37. Aslan K, Wu M, Lakowicz JR, Geddes CD (2007) Fluorescent core −shell Ag@SiO_2 nanocomposites for metal-enhanced fluorescence and single nanoparticle sensing platforms. J Am Chem Soc 129(6): 1524–1525
38. Murray CB, Norris DJ, Bawendi MG (1993) Synthesis and characterization of nearly monodisperse CdE (E = sulfur, selenium, tellurium) semiconductor nanocrystallites. J Am Chem Soc 115(19): 8706–8715
39. Murray CB, Kagan CR (2000) Synthesis and characterization of monodisperse nanocrystals and close-packed nanocrystal assemblies. Annu Rev Mater Res 30(1):545–610
40. Stoeva S, Klabunde KJ, Sorensen CM, Dragieva I (2002) Gram-scale synthesis of monodisperse gold colloids by the solvated metal atom dispersion method and digestive ripening and their organization into two- and three-dimensional structures. J Am Chem Soc 124(10):2305–2311
41. Grzelczak M, Pérez-Juste J, Mulvaney P, Liz-Marzán LM (2008) Shape control in gold nanoparticle synthesis. Chem Soc Rev 37(9): 1783–1791
42. Tao AR, Habas S, Yang P (2008) Shape control of colloidal metal nanocrystals. Small 4(3):310–325
43. Xia Y, Xiong Y, Lim B, Skrabalak SE (2009) Shape-controlled synthesis of metal nanocrystals: simple chemistry meets complex physics? Angew Chem Int Ed 48(1):60–103
44. Chen HY, Lin MH, Wang CY, Chang YM, Gwo S (2015) Large-scale hot spot engineering for quantitative SERS at the single-molecule scale. J Am Chem Soc. doi:10.1021/jacs.5b09111
45. Bantz KC, Meyer AF, Wittenberg NJ, Im H, Kurtulus Ö, Lee SH, Lindquist NC, Oh SH, Haynes CL (2011) Recent progress in SERS biosensing. Phys Chem Chem Phys 13(24):11551–11567
46. Lane LA, Qian X, Nie S (2015) SERS nanoparticles in medicine: from label-free detection to spectroscopic tagging. Chem Rev 115(19):10489–10529
47. Wu X, Ming T, Wang X, Wang P, Wang J, Chen J (2010) High-photoluminescence-yield gold nanocubes: for cell imaging and photothermal therapy. ACS Nano 4(1):113–120
48. Zheng J, Zhang C, Dickson RM (2004) Highly fluorescent, water-soluble, size-tunable gold quantum dots. Phys Rev Lett 93(7): 077402
49. Faraday M (1857) The bakerian lecture: experimental relations of gold (and other metals) to light. Philos Trans R Soc Lond 147:145–181
50. Mie G (1908) Beiträgezur optiktrüber medien, speziellkolloidaler metallösungen. Ann Phys 330(3):377–445
51. Gans R (1915) Form of ultramicroscopic particles of silver. Ann Phys 47:270–284
52. Sudeep PK, Shibu Joseph ST, Thomas KG (2005) Selective detection of cysteine and glutathione using gold nanorods. J Am Chem Soc 127(18):6516–6517
53. Zhang S, Kou X, Yang Z, Shi Q, Stucky GD, Sun L, Wang J, Yan C (2007) Nanonecklaces assembled from gold rods, spheres, and bipyramids. Chem Commun (18):1816–1818
54. Wang L, Zhu Y, Xu L, Chen W, Kuang H, Liu L, Agarwal A, Xu C, Kotov NA (2010) Side-by-side and end-to-end gold nanorod assemblies for environmental toxin sensing. Angew Chem Int Ed 49 (32):5472–5475
55. Wang Y, Li YF, Wang J, Sang Y, Huang CZ (2010) End-to-end assembly of gold nanorods by means of oligonucleotide–mercury (II) molecular recognition. Chem Commun 46(8):1332–1334
56. Huang H, Qu C, Liu X, Huang S, Xu Z, Zhu Y, Chu PK (2011) Amplification of localized surface plasmon resonance signals by a gold nanorod assembly and ultra-sensitive detection of mercury. Chem Commun 47(24):6897–6899
57. Wang J, Zhang P, Li CM, Li YF, Huang CZ (2014) A highly selective and colorimetric assay of lysine by molecular-driven gold nanorods assembly. Biosens Bioelectron 34(1):197–201
58. Wang C, Chen Y, Wang T, Ma Z, Su Z (2007) Biorecognition-driven self-assembly of gold nanorods: a rapid and sensitive approach toward antibody sensing. Chem Mater 19(24):5809–5811
59. Zhen SJ, Huang CZ, Wang J, Li YF (2009) End-to-end assembly of gold nanorods on the basis of aptamer-protein recognition. J Phys Chem C 113(52):21543–21547
60. Lu L, Xia Y (2015) Enzymatic reaction-modulated gold nanorod end-to-end self-assembly for ultrahigh sensitively colorimetric sensing of cholinesterase and organophosphate pesticides in human blood. Anal Chem 87(16):8584–8591
61. Yu C, Irudayaraj J (2007) Multiplex biosensor using gold nanorods. Anal Chem 79(2):572–579
62. Marinakos SM, Chen S, Chilkoti A (2007) Plasmonic detection of a model analyte in serum by a gold nanorod sensor. Anal Chem 79 (14):5278–5283

63. Nusz GJ, Marinakos SM, Curry AC, Dahlin A, Höök F, Wax A, Chilkoti A (2008) Label-free plasmonic detection of biomolecular binding by a single gold nanorod. Anal Chem 80(4):984–989
64. Chen S, Zhao Q, Liu F, Huang H, Wang L, Yi S, Zeng Y, Chen Y (2013) Ultrasensitive determination of copper in complex biological media based on modulation of plasmonic properties of gold nanorods. Anal Chem 85(19):9142–9147
65. Rex M, Hernandez FE, Campiglia AD (2006) Pushing the limits of mercury sensors with gold nanorods. Anal Chem 78(2):445–451
66. Liu X, Zhang S, Tan P, Zhou J, Huang Y, Nie Z, Yao S (2013) A plasmonic blood glucose monitor based on enzymatic etching of gold nanorods. Chem Commun 49(18):1856–1858
67. Zhang Z, Chen Z, Pan D, Chen L (2015) Fenton-like reaction-mediated etching of gold nanorods for visual detection of Co^{2+}. Langmuir 31(1):643–650
68. Zhang Z, Chen Z, Chen L (2015) Ultrasensitive visual sensing of molybdate based on enzymatic-like etching of gold nanorods. Langmuir 31(33):9253–9259
69. Chen Z, Zhang Z, Qu C, Pan D, Chen L (2012) Highly sensitive label-free colorimetric sensing of nitrite based on etching of gold nanorods. Analyst 137(22):5197–5200
70. Agarwal A, Lilly GD, Govorov AO, Kotov NA (2008) Optical emission and energy transfer in nanoparticle−nanorod assemblies: potential energy pump system for negative refractive index materials. J Phys Chem C 112(47):18314–18320
71. Liang GX, Pan HC, Li Y, Jiang LP, Zhang JR, Zhu JJ (2009) Near infrared sensing based on fluorescence resonance energy transfer between Mn:CdTe quantum dots and Au nanorods. Biosens Bioelectron 24(12):3693–3697
72. Xia Y, Song L, Zhu C (2011) Turn-on and near-infrared fluorescent sensing for 2,4,6-trinitrotoluene based on hybrid (gold nanorod) −(quantum dots) assembly. Anal Chem 83(4):1401–1407
73. Wang S, Riahi R, Li N, Zhang DD, Wong PK (2015) Single cell nanobiosensors for dynamic gene expression profiling in native tissue microenvironments. Adv Mater. doi:10.1002/adma.201502814
74. Yuan F, Chen H, Xu J, Zhang Y, Wu Y, Wang L (2014) Aptamer-based luminescence energy transfer from near-infrared-to-near-infrared up-converting nanoparticles to gold nanorods and its application for the detection of thrombin. Chem Eur J 20(10):2888–2894
75. Chen G, Jin Y, Wang L, Deng J, Zhang C (2011) Gold nanorods-based FRET assay for ultrasensitive detection of Hg^{2+}. Chem Commun 47(46):12500–12502
76. Wang L, Jin Y, Deng J, Chen G (2011) Gold nanorods-based FRET assay for sensitive detection of Pb^{2+} using 8-17 DNAzyme. Analyst 136(24):5169–5174
77. Li X, Qian J, Jiang L, He S (2009) Fluorescence quenching of quantum dots by gold nanorods and its application to DNA detection. Appl Phys Lett 94(6):063111
78. Zeng Q, Zhang Y, Liu X, Tu L, Kong X, Zhang H (2012) Multiple homogeneous immunoassays based on a quantum dots-gold nanorods FRET nanoplatform. Chem Commun 48(12):1781–1783
79. Jin R, Cao YW, Mirkin CA, Kelly KL, Schatz GC, Zheng JG (2001) Photoinduced conversion of silver nanospheres to nanoprisms. Science 294(5548):1901–1903
80. Zhang Q, Li N, Goebl J, Lu Z, Yin Y (2011) A systematic study of the synthesis of silver nanoplates: is citrate a "magic" reagent? J Am Chem Soc 133(46):18931–18939
81. Chen L, Ji F, Xu Y, He L, Mi Y, Bao F, Sun B, Zhang X, Zhang Q (2014) High-yield seedless synthesis of triangular gold nanoplates through oxidative etching. Nano Lett 14(12):7201–7206
82. Wu T, Li YF, Huang CZ (2009) Selectively colorimetric detection of cysteine with triangular silver nanoprisms. Chin Chem Lett 20 (5):611–614
83. Chen L, Fu X, Lu W, Chen L (2013) Highly sensitive and selective colorimetric sensing of Hg^{2+} based on the morphology transition of silver nanoprisms. ACS Appl Mater Interface 5(2):284–290
84. Malile B, Chen JIL (2013) Morphology-based plasmonic nanoparticle sensors: controlling etching kinetics with target-responsive permeability gate. J Am Chem Soc 135(43):16042–16045
85. Yang X, Yu Y, Gao Z (2014) A highly sensitive plasmonic DNA assay based on triangular silver nanoprism etching. ACS Nano 8(5): 4902–4907
86. Liang J, Yao C, Li X, Wu Z, Huang C, Fu Q, Lan C, Cao D, Tang Y (2015) Silver nanoprism etching-based plasmonic ELISA for the high sensitive detection of prostate-specific antigen. Biosens Bioelectron 69:128–134
87. Wang X, Li S, Zhang P, Lv F, Liu L, Li L, Wang S (2015) An optical nanoruler based on a conjugated polymer silver nanoprism pair for label-free protein detection. Adv Mater. doi:10.1002/adma.201502880
88. Chan YH, Chen J, Liu Q, Wark SE, Son DH, Batteas JD (2010) Ultrasensitive copper(II) detection using plasmon-enhanced and photo-brightened luminescence of CdSe quantum dots. Anal Chem 82(9):3671–3678
89. Rodríguez-Lorenzo L, Rica R, Álvarez-Puebla RA, Liz-Marzán LM, Stevens MM (2012) Plasmonic nanosensors with inverse sensitivity by means of enzyme-guided crystal growth. Nat Mater 11 (7):604–607
90. Chen H, Xia Y (2014) Compact hybrid (gold nanodendrite-quantum dots) assembly: plasmon enhanced fluorescence-based platform for small molecule sensing in solution. Anal Chem 86 (22):11062–11069
91. Halder A, Ravishankar N (2007) Ultrafine single-crystalline gold nanowire arrays by oriented attachment. Adv Mater 19(14):1854–1858
92. Chen J, McLellan JM, Siekkinen A, Xiong Y, Li ZY, Xia Y (2006) Facile synthesis of gold−silver nanocages with controllable pores on the surface. J Am Chem Soc 128(46):14776–14777
93. Feng Y, He J, Wang H, Tay YY, Sun H, Zhu L, Chen H (2012) An unconventional role of ligand in continuously tuning of metal–metal interfacial strain. J Am Chem Soc 134(4):2004–2007
94. Shi P, Liu Z, Dong K, Ju E, Ren J, Du Y, Li Z, Qu X (2014) A smart "sense-act-treat" system: combining a ratiometric pH sensor with a near infrared therapeutic gold nanocage. Adv Mater 26(38):6635–6641
95. Lakowicz JR (2005) Radiative decay engineering 5: metal-enhanced fluorescence and plasmon emission. Anal Biochem 337 (2):171–194
96. Li Z, Zhu Z, Liu W, Zhou Y, Han B, Gao Y, Tang Z (2012) Reversible plasmonic circular dichroism of Au nanorod and DNA assemblies. J Am Chem Soc 134(7):3322–3325
97. Liu D, Chen W, Wei J, Li X, Wang Z, Jiang X (2012) A highly sensitive, dual-readout assay based on gold nanoparticles for organophosphorus and carbamate pesticides. Anal Chem 84(9):4185–4191